

Hidden Effects of Negative Stacking Fault Energies in Complex Concentrated Alloys

Pei, Zongrui; Dutta, Biswanath; Körmann, Fritz; Chen, Mingwei

DOI

[10.1103/PhysRevLett.126.255502](https://doi.org/10.1103/PhysRevLett.126.255502)

Publication date

2021

Document Version

Final published version

Published in

Physical Review Letters

Citation (APA)

Pei, Z., Dutta, B., Körmann, F., & Chen, M. (2021). Hidden Effects of Negative Stacking Fault Energies in Complex Concentrated Alloys. *Physical Review Letters*, 126(25), Article 255502. <https://doi.org/10.1103/PhysRevLett.126.255502>

Important note

To cite this publication, please use the final published version (if applicable). Please check the document version above.

Copyright

Other than for strictly personal use, it is not permitted to download, forward or distribute the text or part of it, without the consent of the author(s) and/or copyright holder(s), unless the work is under an open content license such as Creative Commons.

Takedown policy

Please contact us and provide details if you believe this document breaches copyrights. We will remove access to the work immediately and investigate your claim.

Hidden Effects of Negative Stacking Fault Energies in Complex Concentrated AlloysZongrui Pei^{*}*Oak Ridge National Laboratory, Oak Ridge, Tennessee 37831, USA*Biswanath Dutta[Ⓜ]*Department of Materials Science and Engineering, Faculty of Mechanical, Maritime and Materials Engineering, Delft University of Technology, Mekelweg 2, 2628 CD Delft, The Netherlands*

Fritz Körmann

*Department of Materials Science and Engineering, Faculty of Mechanical, Maritime and Materials Engineering, Delft University of Technology, Mekelweg 2, 2628 CD Delft, The Netherlands
and Computational Materials Design, Max-Planck-Institut für Eisenforschung GmbH, D-40237 Düsseldorf, Germany*

Mingwei Chen

Department of Materials Science and Engineering and Hopkins Extreme Materials Institute, Johns Hopkins University, Baltimore, Maryland 21218, USA

(Received 21 March 2021; accepted 20 May 2021; published 21 June 2021)

Negative stacking fault energies (SFEs) are found in face-centered cubic high-entropy alloys with excellent mechanical properties, especially at low temperatures. Their roles remain elusive due to the lack of *in situ* observation of nanoscale deformation. Here, the polymorphism of Shockley partials is fully explored, assisted by a new method. We show negative SFEs result in novel partial pairs as if they were in hexagonal close-packed alloys. The associated yield stresses are much higher than those for other mechanisms at low temperatures. This generalizes the physical picture for all negative-SFE alloys.

DOI: [10.1103/PhysRevLett.126.255502](https://doi.org/10.1103/PhysRevLett.126.255502)

Low to negative stacking fault energies (SFEs) are frequently found for high-entropy alloys (HEAs) in theory, particularly for the alloys with excellent mechanical properties such as CoCrFeNiMn [1–4] and CoCrNi [5–9]. Negative SFEs are difficult to identify in experiment, but their existence is indicated by the rich twin and various close-packed nanostructures [10]. In theory, Ising models connect the negative SFEs with the lower energy of a hexagonal close-packed (hcp) structure relative to a face-centered cubic (fcc) structure [11]. For example, the hcp Cantor alloy (CoCrFeNiMn) is indeed thermodynamically more stable than the fcc one at cryogenic temperatures [12]. Alloys are usually synthesized at high temperatures when the fcc structure is more stable than the hcp structure and then quenched down to room or cryogenic temperatures where the stability is probably reversed. The phase transition from fcc to hcp can be kinetically too slow to see. However, the hcp phases under high pressures are indeed formed and retained in CoCrFeNiMn [13,14] and CoCrFeNi [15] even when the pressures were removed. It is widely acknowledged that low to negative SFEs usually result in wide stacking faults (SFs) and large distances between partial dislocations. The mechanical implications of low SFEs have been studied [16,17], but those of negative SFEs are still elusive and urgently need further experimental [18] and theoretical explorations.

Partial dislocations can shape the microstructure and mechanical properties of fcc materials. The abundant Shockley partials and their polymorphism in these HEAs request all intrinsic geometric freedoms (see details below) for a complete description of dislocation geometry. Here, we propose a new notation system that can unambiguously describe all possible dislocation geometries. Assisted by it, our theoretical analysis shows a large SF width is not the only effect of negative SFEs but one of them. The other consequences include a novel dislocation geometry similar to a dissociated dislocation in an hcp structure [Figs. 1, (d), Case C], where the two partials switch their positions in Case O. It is similar to the Lomer-Cottrell lock but with partials on the same slip plane. The special situation of Case C, i.e., when the coupled partials are far away, is common in fcc materials with negative SFEs that include HEAs. It is fundamentally interesting to check whether this new mechanism plays a role in the excellent mechanical properties of HEAs. This mechanistic study is based on a new density functional theory (DFT)-informed multiple-equal-fraction-dislocation (MEFD) formulation [19] and two solute solution strengthening models [16,17].

Full exploration for novel dislocation geometry by a new notation system.—The extremely plentiful configurations of the partials are exemplified by CoCrNi [20,21], CoCrFeNiMn [20], and Al_{0.1}CoCrFeNi [22] in Fig. 1(a).

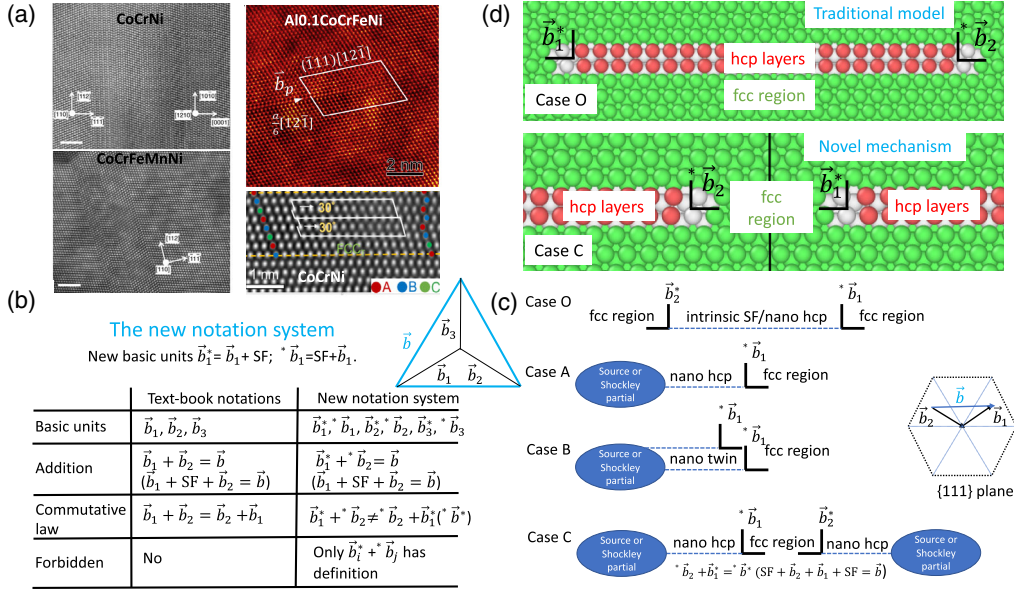


FIG. 1. Full exploration for novel dislocation geometry by a new notation system. (a) Nanoscale close-packed stackings formed by partial dislocation motions are exemplified by CoCrNi [20,21], CoCrFeNiMn [20], and $\text{Al}_{0.1}\text{CoCrFeNi}$ [22]. The profuse partials are highlighted. (b) The new notation system and its comparison with the text-book notion. (c) Four possible configurations of Shockley partials in fcc concentrated alloys. The blue arrows indicate the Burgers vectors of Shockley partials. (d) The configurations of Case C and Case O are illustrated with atomic resolution.

Their geometries cannot be definitely described by Burgers vector only, where the positions of the SFs relative to the partials are ignored. This text-book notation system works well for alloys of positive SFEs, since the relative positions of two partials and one SF are always well-defined. Problems arise when partials are abundant and unbound when SFEs are extremely low to negative. There are three intrinsic geometric freedoms needed for a definite description of an arbitrary number of partials: (i) Burgers vectors \vec{b}_i , (ii) line directions \vec{s}_i , and (iii) the position of partials relative to the SFs. The choice of Burgers vectors is described by the Thompson's tetrahedron; the line direction is in principle arbitrary if symmetry permits; both can be clearly described by the text-book notation system. However the relative positions of the partials is not defined, which is indispensable for alloys with negative SFEs.

A new notation system is proposed here for a complete description of the extremely diverse dislocation geometries [Fig. 1(b)]. The new symbol combines the Burgers vector of a partial and the SF position. For example, when an SF is to the right of the partial \vec{b}_1 , we denote it by \vec{b}_1^* , $\vec{b}_1^* = \vec{b}_1 + \text{SF}$; when it is to the left, $^*\vec{b}_1 = \text{SF} + \vec{b}_1$. [The properties of the new notation system and its applications to describe cases in Fig. 1(c) and beyond are provided in the Supplemental Material [23].] The new system considers all intrinsic geometric freedoms in a simple manner, but the impact is profound. It is useful to describe a more complex geometry in which three or more partial dislocations are involved. The line direction \vec{s} is arbitrary in theory. A general discussion of arbitrary directions is straightforward

but outside the scope of this work. Here, we only consider the two partials with the same line direction.

The new building blocks of starred Burgers vectors (partials) double in number, which greatly increases the possibilities of combinations of partials. We can mechanically play with the building blocks to find a new geometry and then check if they can be a new mechanism with physical meaning. Arguably the easiest way to find a new geometry is to switch the positions of partials in known configurations. For example, we can switch the two partials in Case A, which results in Case C [Fig. 1(c)]. This is similar to a dissociated dislocation in an hcp structure, which can exist in alloys with negative SFEs. As a new type of dislocation geometry in fcc structures, it provides the basis to understand deformation behavior.

The broken equilibrium: Case O.—In the classic Case O, three forces determine the distance between the two Shockley partials, i.e., the interactions of edge components $F_e(x)$, screw components $F_s(x)$, and the attractive force through SFEs $F_\gamma(x)$. Assuming \vec{b}_1^* , $^*\vec{b}_2$ are the Burgers vectors of the two partial dislocations, \vec{s} is the line direction of the whole dislocation, G is the shear modulus along the Burgers vector \vec{b} of the whole dislocation, and ν is the Poisson ratio, we have $F_e = [G/2\pi(1-\nu)](1/x)$ ($\vec{b}_1^* \times \vec{s})(^*\vec{b}_2 \times \vec{s}) > 0$, $F_s = (G/2\pi)(1/x)(\vec{b}_1^* \cdot \vec{s})(^*\vec{b}_2 \cdot \vec{s}) < 0$, and $F_\gamma = -x\gamma_0 < 0$. Here, γ_0 represents the SFE. The equilibrium distance x_0 is calculated by

$$F_e(x_0) + F_s(x_0) + F_\gamma(x_0) = 0. \quad (1)$$

When the SFE is negative, i.e., $F_\gamma = -x\gamma_0 > 0$, the force associated with the SFE becomes repulsive and has the same sign as F_e . The equilibrium of Eq. (1) is, however, broken. The only attractive force from the screw component, F_s , is smaller than F_e , but there is an extra repulsive force term from the SFE. The total force is thus

$$F_e(x) + F_s(x) + F_\gamma(x) > 0. \quad (2)$$

Obviously, there is no solution for x . We will confirm this information again from the numerical solution of a revised Peierls-Nabarro model.

When Shockley partials are profuse, it is possible that one of the partials has a pure screw character. For example, when the right partial is purely screw with the SF to its left (*b_3), $F_e = 0$, we can find a new equilibrium distance $x_0 = -F_s/\gamma_0$. An equivalent case is when the left partial is a screw dislocation, which yields the same equilibrium distance. Here, we focus on a special case, i.e., when the two partials have mixed characters but meet each other from an opposite direction.

The new equilibrium: Case C.—The huge number of partials may meet each other and form new couples in the configuration of Case C [Fig. 1(c), (d), Case C], which can be expressed by $^*b_1 + \vec{b}_2^* = \vec{b}^*$. The configuration of Case C is similar to the dissociated basal $\langle a \rangle$ dislocation on the basal plane in hcp if the principle of nearsightedness is adopted. Transforming the Case C in fcc into the hcp basal $\langle a \rangle$ dislocation with the bulk hcp energy as the new zero energy reference, we again have a positive SFE and the associated force $F_\gamma = -x\gamma_0 < 0$. The new equilibrium distance would be $x_0 = (Gb/\gamma_0)(b/24\pi)[(2+\nu)/(1-\nu)]$ [consequence of Eq. (1)]. Unlike Case O, here the shear modulus G and Poisson ratio ν of hcp rather than fcc are needed, assuming that a dislocation can only feel the interactions of its nearest-neighbor layers. This assumption has been adopted for dislocation-solution interactions [49,50]. The Poisson ratios of the hcp and fcc structures are stably close to 0.3, particularly for the materials with the same constitutions and crystal structures. With the above preparation, Case C in fcc materials can be transformed into Case O in hcp ones. The great advantage of this transformation is (i) the minus sign of the SFE can be dropped and (ii) the dislocation geometry of Case C can be evaluated by classic dislocation theory.

Higher yield stresses in Case C indicated by generalized SFEs.—A generalized SFE (GSFE) is a very useful concept associated with SFEs that provides insights into the mechanical properties. Accurate GSFEs are calculated by DFT (Fig. 2), which can be used to fit the five-point γ surface [24] or its simplified two-point expression $\gamma(x) = \gamma_0 \sin^2(\pi x) + (\gamma_u - \gamma_0/2) \sin^2(2\pi x)$, where γ_0, γ_u are the stable and unstable SFEs. This expression can be

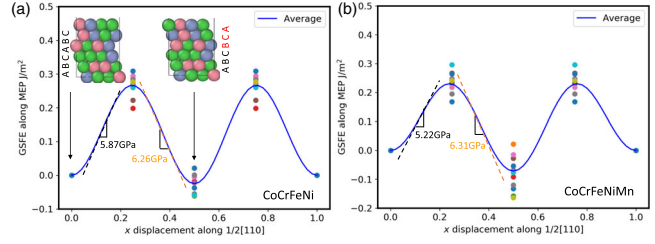


FIG. 2. The minimum energy paths for dislocation motions. Minimum energy paths of GSFEs for (a) CoCrFeNi and (b) CoCrFeNiMn. The insets in (a) illustrate the atomic arrangements before and after Shockley partial glides, the geometries of which are the same for CoCrFeNiMn albeit with different atomic occupations. For both alloys, the maximum shear stress in Case C (right slope, dashed line in yellow) is larger than in Case O (left slope, dashed line in black), indicating a higher yield stress of Case C than the classic one.

easily used to evaluate the effect of SFEs on dislocation geometry and strengthening. Also, the shear modulus can be well evaluated by the slopes of GSFE curves, which are substantially different for hcp and fcc [12]. For Case O, a Shockley partial has to overcome the barrier along the direction $x = 0$ to $1/4$; while for Case C, a larger barrier of the reversed direction has to be overcome. The GSFE curves of hcp and fcc show that the “valley” is deeper for hcp partials than for fcc ones (arrows in Fig. 2), indicating a larger critical resolved shear stress (CRSS) of Case C than Case O.

The γ surface or GSFE curve is reconstructed for Case C. Two steps are needed: (i) drop the minus sign of the SFE, and (ii) add an SFE to the unstable SFEs γ_u . Step (i) is based on ANNNI models, which state that the SFEs for the intrinsic SF I_1 in hcp [51] and the intrinsic SF in fcc are

$$\gamma_{\text{hcp}} \approx -4J_1 + 4J_2 - 4J_3 \approx -4J_1 - 4J_3, \quad (3a)$$

$$\gamma_{\text{fcc}} \approx 4J_1 + 4J_3 \approx -\gamma_{\text{hcp}}. \quad (3b)$$

The extensive data of Hu *et al.* shows J_2 is about $J_1/10$ to $J_1/3$ [52]. As a reasonable approximation, $\gamma_{\text{hcp}} \approx -\gamma_{\text{fcc}}$. This results in two coupled correspondences, i.e., (i) a negative SFE in hcp corresponds to a positive one in fcc and (ii) a negative SFE in fcc corresponds to a positive one in hcp. The above idea allows us to treat an fcc problem with a negative SFE as an hcp one with a positive SFE. This finding directly attributes the different yield stresses of Cases O and C to the different shear moduli of fcc and hcp phases.

Dislocation geometry by MEFD calculations.—It is not convenient to simulate the atomic structure of Case C using atomistic simulations or DFT, since the fcc matrix is less stable than hcp at zero K. We use a revised Peierls-Nabarro model with the MEFD formulation for this purpose. The most important input for the model is the γ surface

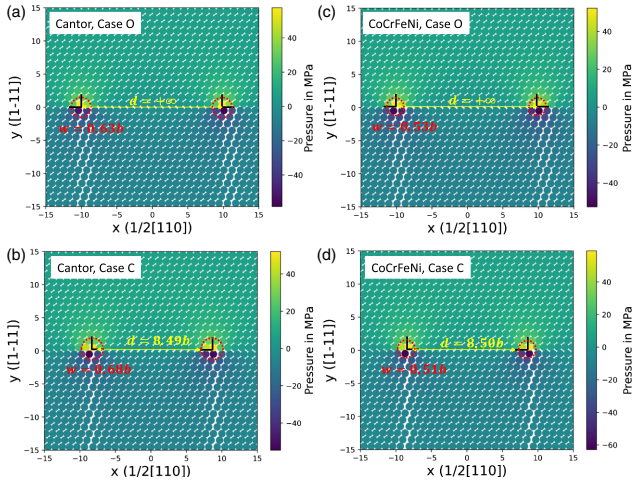


FIG. 3. The dislocation cores computed by a revised Peierls-Nabarro model. Both the classic [(a),(c)] and new [(b),(d)] configurations of Shockley partials in the Cantor and CoCrFeNi alloys are calculated. The partial distance of the classic configuration (Case O) is theoretically infinite, which is reset as $10b$ for better visualization.

introduced in the preceding section. The MEFD formulation is used to solve the Peierls-Nabarro equation [19], which has been successfully used to study Mg [19], HEAs [53], and two-dimensional materials [25]. A total of seven parameters are optimized using the particle swarm optimization algorithm [11,24,26] that has been implemented in the dislocation-simulation toolkit [27].

Figure 3 shows the optimized dislocation core geometry using DFT-computed GSFEs and elastic constants. The core structures in the new Case C are different from the structure in the classic Case O due to the dominant attractive interaction between partials. In Case O, the interaction is either negligible or repulsive. The geometric difference is more significant in Cantor alloy than in CoCrFeNi. For Cantor alloy, the half-width w of each partial in Case C is slightly wider than the half-width w in Case O. The equilibrium distance between partials for both alloys in Case C is about 8.5 Burgers vector; while for Case O, the distance is theoretically infinite, which is consistent with the classic analytical model.

Mechanical consequences of the novel mechanism and magnetic states.—The GSFE curves indicate Case C has a higher CRSS than the classic Case O. Here we directly evaluate their mobility using two widely accepted models. The influence of magnetic states, which are sensitive to the local arrangements of the close-packed planes, is also discussed. Okamoto *et al.* [17] found that the yield stress normalized by shear modulus G for a given alloy follows a rule $\sigma_y/G = k \cdot \text{MSAD}^{1/2}$, where $k \approx 1.3 \times 10^{-3}$ MPa/pm for fcc HEAs, and MSAD represents the mean square atomic displacement. The rule can be recast into $\sigma_y/(k \cdot \text{MSAD}^{1/2}) = G$. For different cases (O, C)

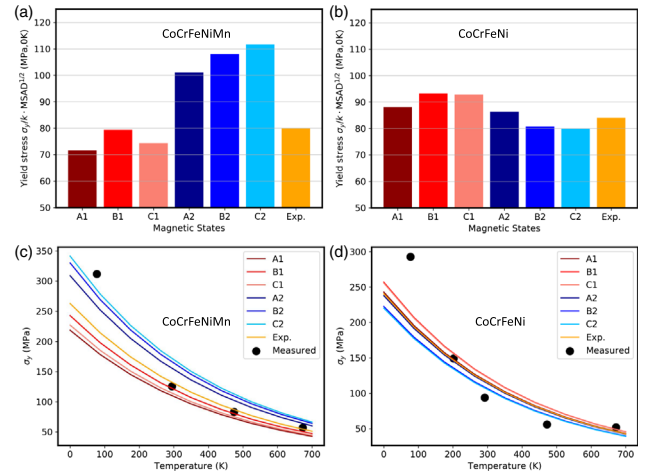


FIG. 4. The mechanical consequences of the new mechanism. The magnetic-state-dependent yield stresses for the new and classic configurations of dislocations, i.e., yield stresses at zero K [(a),(b)] and at finite temperatures [(c),(d)]. The letters represent magnetic states, and the numbers are for different cases (O and C): A-Ferrimagnetic, B-Antiferromagnetic, C-Paramagnetic; 1-Case O, 2-Case C. Both measured yield stresses (dots) and calculated ones using experimental elastic constants (yellow line, “Exp.”) are presented.

and different magnetic states, G or equivalently $\sigma_y/(k \cdot \text{MSAD}^{1/2})$ is different. (See the Supplemental Material [23] for computational details.) The shear moduli G are calculated by bulk moduli and a Poisson ratio of 0.3. The rescaled yield stresses $\sigma_y/(k \cdot \text{MSAD}^{1/2})$ for the six different situations are shown in Fig. 4. The magnetic states substantially change the rescaled yield stresses in both Cases O and C. The most significant feature is that Case C (A2,B2,C2) offers a much higher yield stress than Case O (A1,B1,C1) for the Cantor alloy, while the experimental value lies in between. In contrast, the yield stresses for the CoCrFeNi alloy in Cases O and C are less different and comparable to the influence of the magnetic states. The strengthening effect of magnetism was discussed in [20]. Here, we directly quantified its effect on yield stresses.

We consider a special situation of Case C when the two partials are far away, which is common in experiment [Fig. 1(a)]. The temperature-dependent yield stresses are calculated for the new mechanism (Case C) in two HEAs (Fig. 4) using the Varvenne model [16]. The new mechanism indeed provides a much larger yield stress than the classic mechanism (Case O) for CoCrFeNiMn. At cryogenic temperatures, a 50% higher yield stress is predicted for Case C (paramagnetic state), which better agrees with the experimental measurement for the alloy. This gives another effect induced by the negative SFES in the HEA, which is intrinsic to the new Shockley pairs. The yield stress is more affected by the different mechanisms but also substantially tuned by the magnetic states. For example, the yield stress of the paramagnetic state is larger than the other

two states in Case C. In contrast, the variance of yield stress due to the new mechanism is comparable to the magnetic states for CoCrFeNi. Further experimental investigations on the probability or density of the new configuration (Case C) are still needed.

In summary, we fully explore the geometric and mechanical implications of negative SFEs in high-entropy alloys and add fundamentally new ingredients to understand their excellent mechanical properties. We identify a new dislocation geometry assisted by a notation system invented here. The new configuration of Shockley partials and its special case are expected to be found for all alloys with negative SFEs, which are systematically studied using state-of-the-art DFT simulations and multiscale models and compared to available experimental measurements. The new dislocation geometry results in a higher yield stress at cryogenic temperatures than the traditional mechanisms for CoCrFeNiMn and agrees better with the experiment, which can be activated below the cross-over temperature of the fcc and hcp free energies. The interplay between the new mechanism and various magnetic states of atoms is directly evaluated, showing that magnetism can substantially tune the magnitudes of yield stresses. Our study demonstrates that negative SFEs provide a new group of mechanisms, in addition to the known effects, such as wide SFs. This generalizes the physical picture and lays the foundation for the design of all novel negative-SFE alloys.

This work was sponsored by the U.S. Department of Energy, Office of Science, Basic Energy Sciences, Materials Science and Engineering Division. B.D. and F.K. gratefully acknowledge funding from the Deutsche Forschungsgemeinschaft (SPP 2006) and from NWO/STW (VIDI Grant No. 15707). M.C. acknowledges the support of U.S. National Science Foundation under grant DMR-1804320. The authors also acknowledge the fruitful discussion with Dr. Duancheng Ma and Dr. Hongwei Sheng.

*Corresponding author.
peizongrui@gmail.com

- [1] B. Cantor, I. Chang, P. Knight, and A. Vincent, Microstructural development in equiatomic multicomponent alloys, *Mater. Sci. Eng. A* **375-377**, 213 (2004).
- [2] B. Gludovatz, A. Hohenwarter, D. Catoor, E. H. Chang, E. P. George, and R. O. Ritchie, A fracture-resistant high-entropy alloy for cryogenic applications, *Science* **345**, 1153 (2014).
- [3] Z. Zhang, M. M. Mao, J. Wang, B. Gludovatz, Z. Zhang, S. X. Mao, E. P. George, Q. Yu, and R. O. Ritchie, Nano-scale origins of the damage tolerance of the high-entropy alloy CrMnFeCoNi, *Nat. Commun.* **6**, 10143 (2015).
- [4] S. Chen, H. S. Oh, B. Gludovatz, S. J. Kim, E. S. Park, Z. Zhang, R. O. Ritchie, and Q. Yu, Real-time observations of trip-induced ultrahigh strain hardening in a dual-phase CrMnFeCoNi high-entropy alloy, *Nat. Commun.* **11**, 826 (2020).
- [5] Z. Wu, H. Bei, G. Pharr, and E. George, Temperature dependence of the mechanical properties of equiatomic solid solution alloys with face-centered cubic crystal structures, *Acta Mater.* **81**, 428 (2014).
- [6] Z. Zhang, H. Sheng, Z. Wang, B. Gludovatz, Z. Zhang, E. P. George, Q. Yu, S. X. Mao, and R. O. Ritchie, Dislocation mechanisms and 3d twin architectures generate exceptional strength-ductility-toughness combination in crconi medium-entropy alloy, *Nat. Commun.* **8**, 14390 (2017).
- [7] Q.-J. Li, H. Sheng, and E. Ma, Strengthening in multi-principal element alloys with local-chemical-order roughened dislocation pathways, *Nat. Commun.* **10**, 1 (2019).
- [8] R. Zhang, S. Zhao, J. Ding, Y. Chong, T. Jia, C. Ophus, M. Asta, R. O. Ritchie, and A. M. Minor, Short-range order and its impact on the CrCoNi medium-entropy alloy, *Nature (London)* **581**, 283 (2020).
- [9] B. Yin, S. Yoshida, N. Tsuji, and W. Curtin, Yield strength and misfit volumes of NiCoCr and implications for short-range-order, *Nat. Commun.* **11**, 2507 (2020).
- [10] W. Guo, Z. Pei, X. Sang, J. D. Poplawsky, S. Bruschi, J. Qu, D. Raabe, and H. Bei, Shape-preserving machining produces gradient nanolaminate medium entropy alloys with high strain hardening capability, *Acta Mater.* **170**, 176 (2019).
- [11] Z. Pei, An overview of modeling the stacking faults in lightweight and high-entropy alloys: Theory and application, *Mater. Sci. Eng. A* **737**, 132 (2018).
- [12] D. Ma, B. Grabowski, F. Krmann, J. Neugebauer, and D. Raabe, *Ab initio* thermodynamics of the CoCrFeMnNi high entropy alloy: Importance of entropy contributions beyond the configurational one, *Acta Mater.* **100**, 90 (2015).
- [13] F. Zhang, Y. Wu, H. Lou, Z. Zeng, V. B. Prakapenka, E. Greenberg, Y. Ren, J. Yan, J. S. Okasinski, X. Liu, Y. Liu, Q. Zeng, and Z. Lu, Polymorphism in a high-entropy alloy, *Nat. Commun.* **8**, 15687 (2017).
- [14] C. L. Tracy, S. Park, D. R. Rittman, S. J. Zinkle, H. Bei, M. Lang, R. C. Ewing, and W. L. Mao, High pressure synthesis of a hexagonal close-packed phase of the high-entropy alloy CrMnFeCoNi, *Nat. Commun.* **8**, 15634 (2017).
- [15] F. X. Zhang, S. Zhao, K. Jin, H. Bei, D. Popov, C. Park, J. C. Neufeind, W. J. Weber, and Y. Zhang, Pressure-induced fcc to hcp phase transition in ni-based high entropy solid solution alloys, *Appl. Phys. Lett.* **110**, 011902 (2017).
- [16] C. Varvenne, A. Luque, and W. A. Curtin, Theory of strengthening in fcc high entropy alloys, *Acta Mater.* **118**, 164 (2016).
- [17] N. L. Okamoto, S. Fujimoto, Y. Kambara, M. Kawamura, Z. M. Chen, H. Matsunoshita, K. Tanaka, H. Inui, and E. P. George, Size effect, critical resolved shear stress, stacking fault energy, and solid solution strengthening in the crmnfeconi high-entropy alloy, *Sci. Rep.* **6**, 35863 (2016).
- [18] S. Wei and C. C. Tasan, Deformation faulting in a metastable cocniw complex concentrated alloy: A case of negative intrinsic stacking fault energy? *Acta Mater.* **200**, 992 (2020).
- [19] Z. Pei and G. M. Stocks, Origin of the sensitivity in modeling the glide behaviour of dislocations, *Int. J. Plast.* **106**, 48 (2018).

- [20] C. Niu, C.R. LaRosa, J. Miao, M.J. Mills, and M. Ghazisaeidi, Magnetically-driven phase transformation strengthening in high entropy alloys, *Nat. Commun.* **9**, 1363 (2018).
- [21] F. Zhang, Y. Ren, Z. Pei, Z. Lu, B. Wang, Y. Xue, X. Cao, K. Du, Y. Yang, B. Li, and M. Chen, Dislocation cooperation for hierarchical deformation in shock-loaded multi-principal element alloys (to be published).
- [22] X. Xu, P. Liu, Z. Tang, A. Hirata, S. Song, T. Nieh, P. Liaw, C. Liu, and M. Chen, Transmission electron microscopy characterization of dislocation structure in a face-centered cubic high-entropy alloy Al_{0.1}CoCrFeNi, *Acta Mater.* **144**, 107 (2018).
- [23] See Supplemental Material, which includes additional technical details to calculate and understand the results in the main text and Refs. [11,19,24–54], at <http://link.aps.org/supplemental/10.1103/PhysRevLett.126.255502>.
- [24] Z. Pei, D. Ma, M. Friák, B. Svendsen, D. Raabe, and J. Neugebauer, From generalized stacking fault energies to dislocation properties: Five-energy-point approach and solid solution effects in magnesium, *Phys. Rev. B* **92**, 064107 (2015).
- [25] Z. Pei, S. Mu, and W. Ming, The local strain distribution in bilayer materials: A multiscale study, *Nanoscale* **12**, 6456 (2020).
- [26] Z. Pei and M. Eisenbach, Acceleration of the particle swarm optimization for PeierlsNabarro modeling of dislocations in conventional and high-entropy alloys, *Comput. Phys. Commun.* **215**, 7 (2017).
- [27] Z. Pei, DIST: A dislocation-simulation toolkit, *Comput. Phys. Commun.* **233**, 44 (2018).
- [28] P. Hohenberg and W. Kohn, Inhomogeneous electron gas, *Phys. Rev.* **136**, B864 (1964).
- [29] W. Kohn and L. J. Sham, Self-consistent equations including exchange and correlation effects, *Phys. Rev.* **140**, A1133 (1965).
- [30] G. Kresse and J. Furthmüller, Efficient iterative schemes for *ab initio* total-energy calculations using a plane-wave basis set, *Phys. Rev. B* **54**, 11169 (1996).
- [31] J.P. Perdew, K. Burke, and M. Ernzerhof, Generalized Gradient Approximation Made Simple, *Phys. Rev. Lett.* **77**, 3865 (1996).
- [32] P. E. Blöchl, Projector augmented-wave method, *Phys. Rev. B* **50**, 17953 (1994).
- [33] H. J. Monkhorst and J. D. Pack, Special points for brillouin-zone integrations, *Phys. Rev. B* **13**, 5188 (1976).
- [34] L. Vitos, H. Skriver, B. Johansson, and J. Kollr, Application of the exact muffin-tin orbitals theory: The spherical cell approximation, *Comput. Mater. Sci.* **18**, 24 (2000).
- [35] L. Vitos, Total-energy method based on the exact muffin-tin orbitals theory, *Phys. Rev. B* **64**, 014107 (2001).
- [36] A. V. Ruban and H.L. Skriver, Screened coulomb interactions in metallic alloys. i. universal screening in the atomic-sphere approximation, *Phys. Rev. B* **66**, 024201 (2002).
- [37] A. V. Ruban, S. I. Simak, P. A. Korzhavyi, and H. L. Skriver, Screened coulomb interactions in metallic alloys. ii. screening beyond the single-site and atomic-sphere approximations, *Phys. Rev. B* **66**, 024202 (2002).
- [38] J.P. Perdew, K. Burke, and M. Ernzerhof, Generalized Gradient Approximation Made Simple, *Phys. Rev. Lett.* **77**, 3865 (1996).
- [39] H. J. Monkhorst and J. D. Pack, Special points for brillouin-zone integrations, *Phys. Rev. B* **13**, 5188 (1976).
- [40] J. Staunton, B. Gyorffy, A. Pindor, G. Stocks, and H. Winter, The disordered local moment picture of itinerant magnetism at finite temperatures, *J. Magn. Magn. Mater.* **45**, 15 (1984).
- [41] B. L. Gyorffy, A. J. Pindor, J. Staunton, G. M. Stocks, and H. Winter, A first-principles theory of ferromagnetic phase transitions in metals, *J. Phys. F* **15**, 1337 (1985).
- [42] P. Soven, Coherent-potential model of substitutional disordered alloys, *Phys. Rev.* **156**, 809 (1967).
- [43] B. L. Gyorffy, Coherent-potential approximation for a non-overlapping-muffin-tin-potential model of random substitutional alloys, *Phys. Rev. B* **5**, 2382 (1972).
- [44] Z. Rao, B. Dutta, F. Körmann, D. Ponge, L. Li, J. He, L. Stephenson, L. Schäfer, K. Skokov, O. Gutfleisch, D. Raabe, and Z. Li, Unveiling the mechanism of abnormal magnetic behavior of fcc high-entropy alloys through a joint experimental-theoretical study, *Phys. Rev. Mater.* **4**, 014402 (2020).
- [45] X. Wu, Z. Li, Z. Rao, Y. Ikeda, B. Dutta, F. Körmann, J. Neugebauer, and D. Raabe, Role of magnetic ordering for the design of quinary twip-trip high entropy alloys, *Phys. Rev. Mater.* **4**, 033601 (2020).
- [46] A. Ferrari, B. Dutta, K. Gubaev, Y. Ikeda, P. Srinivasan, B. Grabowski, and F. Körmann, Frontiers in atomistic simulations of high entropy alloys, *J. Appl. Phys.* **128**, 150901 (2020).
- [47] F. Birch, The effect of pressure upon the elastic parameters of isotropic solids, according to murnaghan's theory of finite strain, *J. Appl. Phys.* **9**, 279 (1938).
- [48] S. Huang, H. Huang, W. Li, D. Kim, S. Lu, X. Li, E. Holmström, S. K. Kwon, and L. Vitos, Twinning in metastable high-entropy alloys, *Nat. Commun.* **9**, 2381 (2018).
- [49] G. P. M. Leyson, W. A. Curtin, L. G. Hector, and C. F. Woodward, Quantitative prediction of solute strengthening in aluminium alloys, *Nat. Mater.* **9**, 750 (2010).
- [50] D. Ma, M. Frik, J. von Pezold, D. Raabe, and J. Neugebauer, Computationally efficient and quantitatively accurate multi-scale simulation of solid-solution strengthening by *ab initio* calculation, *Acta Mater.* **85**, 53 (2015).
- [51] S. Sandlöbes, M. Friák, S. Zaeferrer, A. Dick, S. Yi, D. Letzig, Z. Pei, L.-F. Zhu, J. Neugebauer, and D. Raabe, The relation between ductility and stacking fault energies in mg and mgy alloys, *Acta Mater.* **60**, 3011 (2012).
- [52] Q.-M. Hu and R. Yang, Basal-plane stacking fault energy of hexagonal close-packed metals based on the Ising model, *Acta Mater.* **61**, 1136 (2013).
- [53] X. Liu, Z. Pei, and M. Eisenbach, Dislocation core structures and peierls stresses of the high-entropy alloy nicofecrmn and its subsystems, *Mater. Des.* **180**, 107955 (2019).